Astron. Astrophys. 353, 186–202 (2000)

ASTRONOMY AND ASTROPHYSICS

High-resolution spectroscopy of ROSAT low-mass pre-main sequence stars in Orion⋆

J.M. Alcalá[1,5], E. Covino[1], G. Torres[2], M.F. Sterzik[3], M.J. Pfeiffer[4], and R. Neuhäuser[6]

[1] Osservatorio Astronomico di Capodimonte, 80131 Napoli, Italy
[2] Harvard-Smithsonian Center for Astrophysics, 60 Garden Street, Cambridge, MA 02138, USA
[3] European Southern Observatory, Casilla 19001, Santiago 19, Chile
[4] Institut für Astronomie und Astrophysik der Universität München, Scheinerstrasse 1, 81679 München, Germany
[5] Instituto Nacional de Astrofísica, Optica y Electrónica, A.P. 51 y 216 C.P. 72000, Puebla, México
[6] Max-Planck-Institut für Extraterrestrische Physik, 85740 Garching, Germany

Received 8 March 1999 / Accepted 18 October 1999

Abstract. High-resolution spectroscopic observations of the lithium-rich stars found on the basis of the ROSAT All-Sky Survey (RASS) in the general direction of the Orion star forming region are presented. Different properties are derived from the spectra and analyzed: i) the equivalent widths of the lithium 6708 Å absorption line have been measured and a revision of spectral types has been performed; ii) radial velocities (RV) and projected rotational velocities, $v \sin i$, have been derived by application of cross-correlation techniques. A relatively large number of spectroscopic binaries and of suspected spectroscopic binary and multiple systems are found among the stars in the sample. Based on the strength of the lithium line with respect to young open cluster ZAMS stars of the same spectral type, the pre-main sequence nature is confirmed for more than 70% of the stars in the sample. The interrelation of the derived observational properties, such as kinematics, lithium abundance, age and projected rotational velocity of the stars in the sample are analyzed also in connection with the spatial location of the objects. In particular, the comparison between the kinematics of the stars and that of the gas, provided by the CO and CS molecular emission observations, reveals different degrees of clustering of the stars with respect to the cloud material and different kinematical groups can be distinguished. The sample of RASS lithium-rich stars found in the general direction of Orion appears to be a mixture of true Orion stars and, possibly, stars belonging to the Gould Belt.

Key words: stars: low-mass, brown dwarfs – stars: pre-main sequence – stars: rotation – techniques: radial velocities – techniques: spectroscopic – X-rays: stars

Send offprint requests to: J.M. Alcalá

⋆ Based on observations carried out at the Calar Alto observatory, the Multiple Mirror Telescope (a joint facility of the Smithsonian Institution and the University of Arizona) and the European Southern Observatory, La Silla, Chile under proposal number 60.C-0170

1. Introduction

Optical follow-up observations of ROSAT All-Sky Survey (RASS) X-ray sources in nearby star forming regions (SFRs) have revealed the existence of numerous active lithium-rich stars (Krautter et al. 1994; Neuhäuser 1997; Walter et al. 1999 and references therein). These stars are found to be distributed throughout the entire studied areas, both on and in the surroundings of the main molecular cloud cores (Alcalá et al. 1995; 1996, Wichmann et al. 1996; Krautter et al. 1997; Neuhäuser et al. 1995; Preibisch et al. 1998). Being found in the general direction of SFRs and because of their spectroscopic similarities with those of the weak T Tauri stars (WTTS) discovered in previous investigations (Walter & Kuhi 1981; Montmerle et al. 1983; Walter et al. 1988; Feigelson & Kriss 1989) based on EINSTEIN X-ray observations in SFRs, the RASS lithium-rich stars have been classified as WTTS. In the studies of RASS X-ray sources in SFRs, as well as in those of the EINSTEIN investigations, the main indication for the PMS nature of the stellar sources is the presence of strong absorption in the Li I 6708 Å resonance line in a late-type spectrum, accompanied by a high level of chromospheric activity. Assuming that the RASS lithium-rich stars are physically associated with the respective SFR, it turns out that they lie well above the zero-age main sequence (ZAMS) and have typical T Tauri ages (Alcalá et al. 1996 and 1997; Wichmann et al. 1997b; Preibisch et al. 1998).

In general terms, a mix of PMS stars currently drifting out of their birthplaces with typical dispersion velocities of 1–3 km s^{-1} and somewhat older stars already dispersed in the field is expected. However, the interpretation of most of all the RASS lithium-rich stars in well known star forming regions as PMS stars (see Alcalá et al. 1995 and 1996, Wichmann et al. 1996, Magazzù et al. 1997) has triggered a lively debate on their origin and interpretation, and different models have been proposed to explain their spatial distribution (Sterzik & Durisen 1995; Feigelson 1996; Ghorti & Batt 1996). Other authors have questioned the extreme youth of these stars and argued that the dispersed X-ray active stars merely represent a foreground

population of active ZAMS (Pleiades-like) stars with characteristic ages of about 100 Myrs (Briceño et al. 1997). Favata et al. (1998) use a sample of active stars showing lithium in their optical spectra and selected from EINSTEIN X-ray survey observations, claiming that their sample is representative of the RASS lithium-rich stars samples. As Favata et al. find that, based on Hipparcos parallaxes, their X-ray selected stars fall on the ZAMS, they conclude that the RASS lithium-rich stars found around SFRs also are ZAMS stars. However, the stars in the Favata et al.'s sample are distributed *everywhere* in the sky, and as confirmed from the SIMBAD data base, almost all of them are in double systems. Such a sample is by no means representative of the RASS lithium-rich stars because, though distributed on wide areas, the RASS samples are still spatially concentrated towards the direction of SFRs where there is a much higher probability of finding X-ray emitting PMS stars than when considering any randomly selected direction of the sky. Yet, those authors still mix up off-cloud PMS stars with field lithium stars.

Hipparcos parallaxes, available only for a minority of the RASS lithium-rich stars, place these objects above the ZAMS in the HR diagram (Neuhäuser & Brandner 1998). Unfortunately, the Hipparcos mission has not solved the problem of the distance determination because most of the RASS lithium-rich stars remained unobserved by Hipparcos. In spite of this, some authors (Bouvier et al. 1997) have assigned the "post T Tauri" (PTTS) status to many RASS lithium-rich stars.

Martín (1997) has proposed a classification scheme for low-mass PMS stars based on the position of the candidate PMS stars in the lithium λ 6708 Å equivalent width versus effective temperature diagram. Such a classification scheme has been applied to many X-ray discovered PMS candidates and several of them have been classified as PTTS (Martín & Magazzù 1999; Martín 1998).

Martín (1997) proposed that PTTS are those lying above the upper envelope of the ZAMS stars, but below another line he has drawn in the lithium equivalent width versus effective temperature diagram. The latter line was empirically defined such that TTS in Taurus are located below this line, according to Martín (1998). Hence, by such definition, the PTTS "gap" in Taurus is empty. However, if one plots all TTS and all highest resolution lithium data in Taurus, such "gap" is not empty (e.g. Neuhäuser et al. 1997).

Another source of uncertainty in establishing the evolutionary stage of the RASS lithium-rich stars is that the lithium strength may be overestimated in mid-resolution spectra because of blending with nearby iron lines (see tables by Walter et al. 1988; Covino et al. 1997). Furthermore, other stellar physical quantities like mass and rotation can affect the Li I λ6708 Å line strength (Soderblom et al. 1993).

Previous studies of PMS star candidate samples in the Chamaeleon and Lupus SFRs (Covino et al. 1997; Wichmann et al. 1999) have clearly shown the effectiveness of high-resolution spectroscopy to characterize the nature of RASS-discovered PMS stars. The discrimination of *bona-fide* PMS stars is operated by means of a *lithium criterion*, based on a measure of the lithium excess with respect to the upper limit for stars in young clusters of similar spectral type, combined with the analysis of the kinematical information provided by radial velocity measurements. Walter et al. (1998) made an unbiased lithium survey in one degree field around the star σ-Orionis and found that the radial velocity distribution of the lithium stars they find, is significantly different from that of field stars in the same sky area. Similar results are found by Dolan and Mathieu (1999) in another unbiased lithium survey in one degree around λ Orionis. Therefore, kinematics and lithium together are strong criteria for the association of PMS stars to SFRs.

Intermediate resolution spectroscopy and photometric follow-up observations of RASS sources in Orion have been reported by Alcalá et al. (1996; hereafter Paper I). Alcalá et al. (1998, hereafter Paper II) have placed a representative sample of these stars on the HR diagram adopting the distance of 460 pc to the Orion SFR. The comparison with D'Antona & Mazzitelli's (1994) PMS evolutionary tracks indicates masses for these stars in the range $0.8 < M_{star}/M_{\odot} < 3.4$ and ages $2 \cdot 10^5$ yr $< \tau_{age} < 7 \cdot 10^6$ yr.

In this paper we report the results for a large sample of the stars reported in Paper I. In Sect. 2 the observations and reductions are described, in Sect. 3 the Hα and Li lines of the sample are discussed. The procedures used for the determination of radial velocities, projected rotational velocities, and effective temperatures from the high-resolution spectra are described in Sect. 4 and the results are reported in Sect. 5. In Sect. 6 we discuss the results and draw our conclusions in Sect. 7.

2. Observations and data reduction

High-resolution spectroscopic observations of the stars in our sample were performed at different observatories using different telescopes and spectrographs. Of the 112 stars in the original sample reported in Paper I, 82 were observed in December 1996, October 1997 and December 1997 using the Fiber Optics Cassegrain Echelle Spectrograph (FOCES) attached to the 2.2m telescope at Calar Alto Observatory in Spain. Some seventy spectral orders are included in these spectra covering a range from 4200 to 7000 Å, with a nominal mean resolving power of $\lambda/\Delta\lambda \approx$ 30,000. Technical details regarding FOCES can be found in Pfeiffer et al. (1998). The reduction of the FOCES spectra has been performed using IDL[1] routines specifically written for this instrument (Pfeiffer et al. 1998). For each night, average calibration frames are calculated and cleaned from spikes produced by cosmic-ray impacts and a dark exposure is subtracted from all the frames. Then, the order positions are searched for and determined by cross-order scans of the mean flat-field. From the dark-corrected images the background is fitted and subtracted. Flat-field and thorium calibration spectra are then extracted and the wavelength dispersion relation is determined for all orders. The resulting spectra are then divided by the corresponding order flat-field. Finally, the one-dimensional spectra are merged and cleaned from the spikes

[1] IDL is a high-level interactive language distributed by Research Systems Inc.

Table 1. Data from the high-resolution spectroscopy. The columns are as follows: (1) ROSAT designation; (2) Spectral type; (3) type of Hα profile; (4) Lithium equivalent width; (5) radial velocity from CA & ESO spectra; (6) radial velocity from CfA spectra; (7) vsini from CA & ESO spectra; (8) vsini from CfA spectra; (9) number of CA, CfA & ESO spectra respectively; (10) Lithium abundance in the $logN(H) = 12$ scale; (11) X-ray luminosity; (12) footnotes to table.

RXJ (1)	SpT (2)	$P_{H\alpha}$ (3)	W(Li) (4) [mÅ]	RV (5) [km/s]	RV (6) [km/s]	vsini (7) [km/s]	vsini (8) [km/s]	Nobs. (9)	$logNLi$ (10)	$logL_X$ (11) erg/s	Notes (12)
0500.4−1054†	K7	3	250±15	12.0±4.0				1, 0	1.67	30.78±0.19	
0501.1+0642	K3	3	400±10	19.5±1.0	19.8±0.7	19	21	2, 3	2.95	30.81±0.17	
0502.4−0744	G6	1	305±10	16.7±1.4	16.3±0.7	21	26	1, 4	3.35	30.99±0.17	VAR?
0503.8−1130	K1	2	360±15	24.0±1.0	24.6±0.9	25	22	1, 2	3.12	30.83±0.18	
0506.2+0439	M3				18.8±2.4		26	0, 2		31.47±0.07	
0507.5+1010†	G8	1	260±10	16.7±1.7	16.3±0.6	40	40	1, 3	3.06	31.43±0.09	
0507.8−0931	K2	2	330±20	19.0±1.7	19.5±2.0	64	60	1, 2		30.96±0.14	SB2?
0509.0−0315†	K1	2	320±8	23.4±2.0	22.6±1.1	41	41	1, 2	2.97	31.08±0.13	a
0510.1−0427†	K4	3	230±10	22.8±0.9	19.9±0.4	13	5	1, 2	2.15	31.26±0.12	
0510.3−0330	G8	2	320±15	19.0±1.8	17.5±1.1	35	36	1, 2	3.27	31.03±0.22	
0511.7−0348	K1	2	370±15	17.7±1.1	14.9±1.3	35	35	1, 2	3.16	30.85±0.33	
0512.3−0255	K1	4	440±10	23.3±1.2	22.0±0.9	34	36	1, 3	3.48	31.09±0.15	
0513.1+0851	K2	3						1,10		30.87±0.16	ST3
0513.4−1244	G4	1	220±15	14.8±1.7	8.8±0.8	58	63	1, 3	3.11	31.22±0.19	
0515.6−0930	G5	1	245±8	21.8±1.0	20.3±0.4	17	18	1, 3	3.22	31.68±0.07	
0517.9−0708†	K2	2	260±8	20.9±0.9	19.5±0.4	17	18	1, 3	2.62	31.22±0.10	
0518.0−1146	K3	3	400±20	16.5±2.2	16.0±1.1	60	60	1, 2	2.95	31.23±0.09	SB?
0518.0+0712	K2	2	410±30	21.4±1.9	23.6±2.0	74	65	2, 2	3.16	30.85±0.18	SB?, a
0518.3+0829†	G7	3	250±5	17.4±0.9	16.0±0.6	15	13	1, 2	3.11	31.25±0.10	
0518.6+0959*	K2	2	370±20	23.2±1.8	21.6±1.9	42	37	1, 3	3.00	30.82±0.16	
0519.9+0552	K7	3	610±10	10.0±1.2	14.3±1.5	35	31	0, 1, 1	2.88	31.15±0.12	d
0520.0+0612	K4	3	470±5	18.7±0.9	19.0±0.2	9	7	1, 3	3.03	31.37±0.10	
0520.5+0616	K4	3	510±8	18.5±1.4	18.0±0.5	17	16	1, 3	3.19	31.51±0.08	
0520.9−0452†	F7	1	200±35	25.9±3.4	23.5±0.6	52	51	1, 6	3.48	30.68±0.18	VAR?, a
0522.1−0844	K0	2	380±10	14.9±1.4	13.4±0.7	18	17	1, 2	3.37	30.95±0.16	
0522.9+0857	G9	3						1,29		31.91±0.06	SB2
0523.0−0850	K7-M0				28.1±1.7		6	0, 1		31.24±0.10	
0523.1−0440	K6	4	540±10	24.8±1.2		10		0, 0,1	2.89	30.98±0.29	
0523.7+0652	K7-M0	3	615±15	18.0±1.9	18.4±1.0	55	55	1, 3	2.55	31.08±0.15	SB?
0524.1+0730	K2	5	490±15	14.3±1.2	12.9±1.8	84	80	1, 3	3.54	30.80±0.22	a
0525.3+0208	M4							0, 0		31.16±0.13	e
0526.5+1510	G5	1	–	22.4±2.6	25.6±4.3	145	150	1, 1	–	30.30±0.24	a, b
0526.7+0143	K0	2	315±10	15.1±1.2	19.0±0.6	27	23	1, 3	3.11	30.73±0.22	SB2?
0526.8+0222	G4	1	220±30	17.6±1.9	17.1±2.5	84	82	1, 2	3.20	31.20±0.14	
0528.0−0053	K1	2						1, 3		30.74±0.19	SB2b, f
0528.3+0326	K0	2	390±10	19.7±2.0	17.5±1.7	50	45	1, 2	3.42	30.99±0.17	SB?, a
0528.8+0048	K0	2						5, 4		30.89±0.16	SB2b
0528.8+0105†	K3	2	250±10	16.3±0.9	17.0±0.3	18	7	1, 3	2.41	30.95±0.11	
0529.2−0615†	G9	2	120±10	13.7±1.2	22.4±0.7	41	42	1, 4	2.44	30.95±0.18	SB1
0529.4+0041	K2	2						1, 1		30.97±0.17	ST3, g
0530.1+0041	G2	1	260±10	25.9±1.6	26.4±0.4	60	65	2,19	3.44	31.70±0.06	VAR?, a
0530.7−0434	K3	3					10	9,10		31.13±0.16	SB2
0530.9+1015*	K3	5	500±30	24.1±2.3	17.8±3.7	150	132	1, 4	3.36	31.22±0.12	SB?, a, b, c
0531.2+0118	K0	3	350±10	22.3±1.0	20.8±0.5	9	8	1, 2	3.24	30.67±0.22	VAR?, h
0531.6−0326†	K0	1	160±5	27.1±0.5	27.3±0.3	12	8	2, 4	2.56	31.26±0.14	
0532.1−0732	K2	3						10,1		30.08±0.17	SB2
0532.2−1340†	F8	1	190±10	19.2±1.8	17.4±1.0	68	72	2, 7	3.41	31.22±0.10	
0532.4+0131a	G9	2	365±10	23.3±1.5	20.8±0.6	23	21	1, 2	3.39	30.71±0.22	VAR?
0532.4+0131b	K4	3	460±10	14.7±1.5	17.5±0.6	17	18	0, 2, 1	2.99	30.71±0.22	
0532.4−0713	K2	3	480±8	27.3±1.1	20.1±0.8	33	31	1, 2	3.49	30.96±0.23	
0532.5−0421	K3	4	495±5	21.5±1.4	28.4±0.6	21	35	1, 3	3.34	30.92±0.15	i

Table 1. (continued)

RXJ (1)	SpT (2)	$P_{H\alpha}$ (3)	W(Li) (4) [mÅ]	RV (5) [km/s]	RV (6) [km/s]	vsini (7) [km/s]	vsini (8) [km/s]	Nobs. (9)	$logNLi$ (10)	$logL_X$ (11) erg/s	Notes (12)
0532.6−0522	K3	4	500±10	29.0±5.5	20.0±7.1	125	144	1, 1	3.36	31.49±0.10	SB?, a,b
0533.1−0758	K1	3	420±10	25.5±1.8	21.7±1.0	47	47	1, 3	3.38	31.00±0.21	
0533.1+0224	K3	3	440±30	19.9±1.5	25.5±1.8	54	63	1, 2	3.10	30.98±0.14	SB?, a
0533.5−0646	G7	5	280±15	27.8±1.6	25.8±1.3	106	113	1, 4	3.20	30.89±0.15	VAR??, b
0534.6+1007	G8	3	330±5	19.8±1.0		25		1, 0	3.31	32.27±0.03	
0534.7−0423	K2				27.2±0.9		20	0, 1		31.16±0.09	
HBC447‡	K1							0,54		31.36±0.13	SB2
0534.7+1114†	K1	2	280±10	23.7±1.0	21.0±0.9	20	19	1, 2	2.83	30.70±0.29	
0535.0−0411	G9	3	360±10	27.0±1.5	30.4±0.4	20	22	2, 3	3.37	30.97±0.14	SB2?
0535.6−0152	G6	1						1, 3		30.56±0.24	SB2b
0535.8−0508	K7							0, 0		31.78±0.05	
0535.3−0059	K3	3	470±8	19.6±1.0	19.1±0.8	24	23	1, 2	3.23	30.60±0.31	
0535.7−0418	K3							0, 0		30.10±0.17	
0536.2−0519	K3							0, 0		30.10±0.17	
0536.7+0907	K2	3	455±10	27.0±1.0	24.6±0.9	28	25	1, 2	3.37	30.80±0.17	
0536.9+0608	K0	1						1, 2		30.10±0.17	SB2b, a, b, c
0537.0−0300	G4	1	217±15	23.8±2.1	25.8±3.1	135	130	1, 2	3.19	31.51±0.08	a, b
0537.6+0054	K1	3	410±10	19.5±1.0	12.3±0.5	27	26	1, 3	3.33	30.77±0.18	
0538.4−0637a	K1	2	235±15	10.9±1.3	18.4±0.5	25	13	1, 3	2.69	31.02±0.14	SB2?
0538.4−0637b	K3	3	420±10	20.5±1.2	17.8±0.4	14	9	0, 3, 1	3.02	31.02±0.14	
0538.6−0856	G7	1	290±10	24.5±1.5	26.2±1.0	30	29	1, 2	3.24	31.75±0.06	
0538.8+1302	K0				21.1±0.5		12	0, 2		29.90±0.17	
0538.9−1321†	G0	1	190±10	20.2±1.5	16.9±1.2	52	52	1, 3	3.29	30.85±0.14	VAR?, a
0538.9−0249	K2				27.8±0.9		28	0, 2		30.85±0.22	
0538.9−0624†	G9	1	140±10	24.5±1.0	22.5±0.4	4	6	1, 2	2.55	31.12±0.18	
0539.2+0101	G4				22.3±0.9		32	0, 2		30.94±0.15	
0539.3+0918	K1	2	400±20	18.8±1.9	30.8±3.4	108	92	1, 2	3.29	30.84±0.19	VAR?, a, b
0539.4−0346	G6	1	325±10	24.6±2.4	23.3±0.6	73	66	1, 6	3.44	30.81±0.15	VAR?, a
0539.6−0242	G5	4	300±20	32.6±3.8	–	150	–	1, 1	3.41	31.09±0.13	b
0539.8−0205	K6	3						1, 1		30.79±0.18	ST3
0539.8−0138	K3	3	530±8	24.3±1.5	21.6±1.1	28	28	1, 2	3.50	30.73±0.18	
0539.9−0443†	G1	1	150±10	24.1±2.0	23.3±1.6	58	45	1, 3	3.11	30.91±0.13	j
0539.9+0915†	K0	2	300±5	20.0±2.0	17.1±0.5	21	19	1, 3	3.05	30.96±0.11	
0539.9+0956	K2							0,23		31.80±0.05	SB1
0540.1−0627	M1							0, 0		30.10±0.17	
0540.1−0737	G5	4	250±10	18.9±1.8	17.7±0.8	39	42	1, 5	3.24	30.98±0.30	VAR?
0540.2−0708	K0	2	250±20	22.2±1.4	22.8±1.0	36	36	1, 3	2.89	29.90±0.17	SB2?
0540.5−0121	K1	3						1, 3		30.89±0.14	SB2b
0540.8−0806	K3				24.4±1.1		57	0, 3		30.99±0.22	SB1
0541.3+0027	K2				25.8±0.9		24	0, 2		30.83±0.12	k
0541.4−0324	K3	2					20	1,10		30.85±0.17	ST3
0541.8+0944	G4	1	230±15	30.3±2.6	30.8±1.1	92	90	1, 3	3.23	30.95±0.18	
0541.9−0556	K5				9.0±2.5		55	0, 1		30.85±0.19	
0542.4−0626	G7	1	320±20	17.6±1.3	10.1±1.7	79	72	1, 3	3.35	30.62±0.24	VAR?, a
0542.7−0925	K0	2	340±15	18.7±1.4	17.6±1.0	46	48	1, 3	3.20	30.87±0.18	SB?
0543.5−0642	K1	2	–	19.4±2.6	23.8±4.5	129	146	1, 2	–	30.57±0.20	
0544.2−0941	G9	1	240±35	19.1±2.6	19.5±1.3	93	84	1, 2	2.94	30.68±0.22	SB?, a, b
0544.2−1306	K1				13.8±1.0		28	0, 2		30.42±0.28	
0544.2+0115†	K3	2	310±10	19.5±1.0	17.8±0.5	17	11	1, 2	2.63	30.76±0.19	
0544.6−0121	K3	2	405±10	28.7±1.5	23.2±0.9	34	32	0, 2, 1	2.95	30.92±0.16	
0545.6−1020	G7				14.8±1.0		86	0, 2		30.82±0.19	
0546.1+1232	G6	5	290±20	23.6±2.0	29.6±2.1	138	142	1, 2	3.30	30.84±0.20	b
0546.7−1223	G5							0, 0		30.68±0.35	
0549.6+0232	K0	2	420±10	26.3±1.7	23.7±1.2	35	35	1, 2	3.57	31.04±0.14	

Table 1. (continued)

RXJ (1)	SpT (2)	$P_{H\alpha}$ (3)	W(Li) (4) [mÅ]	RV (5) [km/s]	RV (6) [km/s]	vsini (7) [km/s]	vsini (8) [km/s]	Nobs. (9)	$logNLi$ (10)	$logL_X$ (11) erg/s	Notes (12)
0551.2−0653	K1				19.5±5.9		176	0, 1		30.93±0.15	b
0552.3−0557	K2				24.6±0.7		8	0, 1		30.81±0.18	
0554.6−0736†	G6	1	210±15	17.4±1.5	15.0±1.5	58	55	0, 2, 1	3.05	30.68±0.23	
0556.1−0800	G8				18.4±2.0		60	0, 2		30.94±0.16	
0556.5+0619	K1				-12.0±0.1		5	0,13		30.84±0.14	SB1
0558.0+0929†	G4	1	200±10	20.7±1.0	17.7±1.0	27	30	1, 2	3.14	30.62±0.22	
0558.0−0145	K2				35.7±0.4		8	0, 2		30.67±0.22	

SB1: single line spectroscopic binary; SB2: double line spectroscopic binary; SB2b: double line spectroscopic binary but the components are partially blended; ST3: spectroscopic triple; SB2?: suspected double line spectroscopic binary; SB?: suspected spectroscopic multiple; VAR?: possibly variable RV.

†: stars falling below or just above the upper envelope of young open clusters.

a: asymmetric cross-correlation function; **b**: broad cross-correlation function; **c**: thin component overimposed to a broad one in the cross-correlation function; **d**: visual companion at 2.5″ SE; **e**: visual companion at 5″; **f**: faint visual companion at 10″ NW; **g**: visual companion at 1″ NE; **h**: visual companion at 2″ NE; **i**: 1″ NS pair; **j**: visual companion at 1″ NW; **k**: visual companion at $< 1''$ NW.

$*$: the results from the CfA spectra for these stars are taken from Neuhäuser et al. (1997)

‡: Optical counterpart of the RASS source RXJ 0534.7−0524.

produced by cosmic-ray impacts. The steps of the reduction of the FOCES spectra are described in more detail in Pfeiffer et al. (1998).

Additionally, high-resolution single-order echelle spectra were obtained at the Center for Astrophysics (CfA) for 101 of the 112 stars of the sample in Paper I, using the Multiple Mirror Telescope (Arizona), the 1.5m Tillinghast reflector (Whipple Observatory, Arizona), and the 1.5m Wyeth reflector at Oak Ridge Observatory (Massachusetts). These observations have a resolving power of $\lambda/\Delta\lambda \approx$ 35,000, and cover a 45 Å wavelength range centered at 5187 Å. The reduction of the CfA spectra was carried out as described in Neuhäuser et al. (1995).

Finally, other 6 stars were observed on February 1998 using the Cassegrain Echelle Spectrograph (CASPEC) attached to the 3.6m telescope of the European Southern Observatory at La Silla, Chile. The data reduction was performed using the Echelle reduction package available within the Munich Image Data Analysis System (MIDAS, version November 1997), plus some specially devised procedures making use of the algorithms prescribed by Verschueren & Hensberge (1990) for background subtraction and optimal order extraction, as described in Covino et al. (1997). The nominal resolving power of these spectra, as measured from several isolated lines of the thorium-argon comparison spectrum, is $\lambda/\Delta\lambda \approx$ 22,000.

Except in a few cases, each star was observed only once with FOCES or CASPEC while typically at least two observations were obtained at CfA. In total, 106 stars of the original sample of the 112 in Paper I have FOCES, CASPEC and/or CfA spectra. Of these, 85 have both CfA and FOCES or CASPEC spectra. In order to make easier the comparison with the original sample, we list in Table 1 the whole sample of the 112 stars of Paper I.

We stress that the sample observed at high-resolution is fully representative of the one reported in Paper I, as no bias was introduced in the selection of the targets with respect to spatial direction or lithium strength as measured on the low-resolution spectra.

The FOCES and CASPEC spectra are used to derive Li equivalent widths, W_{hr}(Li) (see Sect. 3.2), as well as radial velocities (RV) and projected rotational velocities ($v \sin i$), while the CfA spectra are used to derive RV and $v \sin i$, and to estimate effective temperatures (Sect. 4).

3. Radial velocity, $v \sin i$, and effective temperature determination

3.1. Radial velocity and $v \sin i$ determinations

Determination of radial velocity, RV, and projected rotational velocity, $v \sin i$ on FOCES and CASPEC spectra, have been obtained by means of cross correlation analysis of the stellar spectra with those of radial velocity and rotational standard stars, treated in analogous way. Given the large spectral range covered by the FOCES and CASPEC spectra, the cross correlation of the target and template stars was performed after rebinning the spectra to a logarithmic wavelength scale, in order to eliminate the dependence of Doppler shift on the wavelength (Simkin, 1974). Moreover, only parts of the spectra free of emission lines and/or not affected by telluric absorption lines have been considered. Therefore, the NaI D, and Hα lines as well as wavelengths longer than about 7000 Å have been excluded from the cross-correlation analysis. The result of the cross-correlation is a correlation peak which can be fitted with a Gaussian curve. The parameters of the Gaussian, center position and full-width at half-maximum (FWHM) are directly related to RV and $v \sin i$, respectively. The method of the correlation has been fully described by Queloz (1994), and Soderblom et al. (1989). More details about the calibration procedure can be found in Appendix A of Covino et al. (1997).

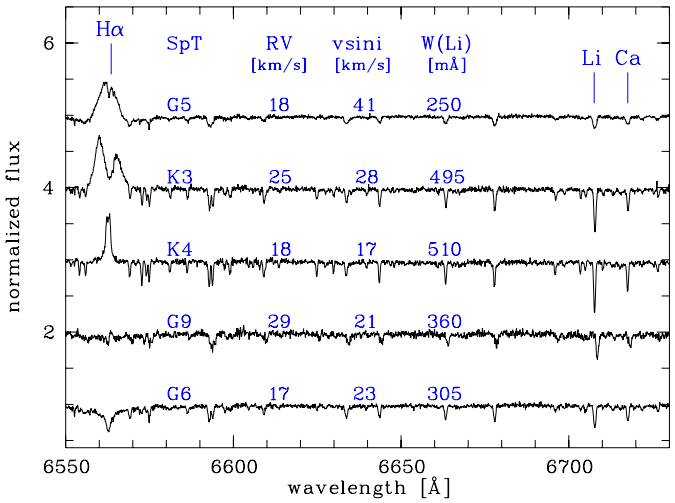

Fig. 1. Typical examples of high-resolution FOCES spectra of the stars in our sample. From the bottom to the top are RXJ0502.4-0744, RXJ0535.0-0411, RXJ0520.5+0616, RXJ0532.5-0421 and RXJ0540.1-737

As a consequence of the Gaussian fit, the cross-correlation method is more reliable for relatively slow rotators. Thus, for faster rotators ($v \sin i$ larger than 40 km s^{-1}) we also applied the Fourier transform analysis to extract the rotational broadening information from spectral line profiles, using the analytical functional form for the rotation profile given by Gray (1976), as already described in Covino et al. (1997). The results obtained with the FFT method and cross correlation technique match pretty well within the errors for intermediate rotational velocities.

Radial velocities from the CfA spectra were obtained for each star also by cross-correlation using the IRAF[2] task XCSAO (Kurtz & Mink 1998). The templates were chosen from an extensive grid of synthetic spectra based on model atmospheres by Kurucz (1992a; 1992b), available for a range of effective temperatures, projected rotational velocities, surface gravities, and metallicities. A large number of correlations were performed for each star to determine the best template. In addition to the radial velocities, we determined the rotational broadening by correlating against templates with a range of values of $v \sin i$, and then interpolating in a table of correlation value versus $v \sin i$ to maximize the average correlation over all exposures of each star.

The RV values as derived from the FOCES and CASPEC and from the CfA spectra are reported in Table 1, Columns 5 and 6 respectively, while the $v \sin i$ values are listed in Columns 7 and 8. The errors on $v \sin i$ are typically of 2 km s^{-1}, for $v \sin i$ less than about 60 km s^{-1}, about 5 km s^{-1} for $60 < v \sin i < 90$, and up to 10 km s^{-1} for faster rotators.

Excluding the spectroscopic multiple systems, the RV and $v \sin i$ values derived from the FOCES and CASPEC are in very good agreement, within the errors, with those derived from the CfA spectra. The average differences are $<$RV(FOCES & CASPEC) $-$ RV(CfA)$>= 0.8 \pm 3.5$ km s^{-1} and $<v \sin i$(FOCES & CASPEC) $- v \sin i$(CfA)$>= 0.9 \pm 5.3$ km s^{-1}, with the largest residuals for the faster rotators.

For the rest of the paper, when more than one measurement exist, we will use the mean of the RV and $v \sin i$values given in Columns 5 & 6 and 7 & 8 of Table 1, respectively.

3.2. T_{eff} determinations

A careful revision of the spectral type classification reported in Paper I was performed using spectral type standards, in a similar way as described in Covino et al. (1997). The new classification leads to the spectral types reported in Table 1. In most cases the previous classification is confirmed and only in a few cases, a difference of a few subclasses is found. The T_{eff} values have then been derived using the spectral types and the spectral type vs. $log\ T_{eff}$ relation for luminosity class V given by de Jager & Nieuwenhuijzen (1987).

In addition we used the CfA spectra to determine effective temperatures by cross-correlation with the grid of synthetic templates described above. The procedure is analogous to that applied to determine $v \sin i$. For further details, the reader is referred to Neuhäuser et al. (1997b).

The second method is somewhat less accurate for stars with lines that are broadened significantly by rotation. In addition, spectra showing two sets of lines (double-line binaries) require a special treatment which is beyond the scope of this paper.

Excluding spectroscopic multiple systems and stars with very broad lines and asymmetries in their cross-correlation peak, the mean difference between T_{eff} derived from the first and second method is $< \Delta T_{eff} >= 70 \pm 190$ K. Therefore, the two methods yield consistent results within the errors. However, for the sake of consistency, we use for the rest of the paper the T_{eff} values derived from the spectral types listed in Table 1.

4. The Hα and the Lithium lines

4.1. Hα line profiles

Typical FOCES spectra in the range from Hα to the Li I(6708 Å) line are shown in Fig. 1. Except for the star RXJ0523.1-0440[3], the Hα emission line equivalent widths of the RASS PMS stars in Orion are all less than 10 Å. The Hα line displays a variety of profiles which can be grouped in four main categories, as the PMS stars in Chamaeleon studied by Covino et al. (1997). The type of Hα line profile is indicated for each star in Column 3 of Table 1, as follows: 1) Hα in absorption; 2) Hα filled in with emission; 3) quite narrow and symmetric (typically chromospheric) Hα emission, and 4) complex Hα line profile (showing

[2] IRAF is distributed by the National Optical Astronomy Observatories, which is operated by the Association of Universities for Research in Astronomy, Inc., under contract with the National Science Foundation.

[3] The Hα equivalent width of this star measured from its high-resolution spectrum is greater than 23 Å, while from the low-resolution spectrum we reported a value of 11.6 Å in Paper I. Therefore, it is likely that this star presented a flare during the high-resolution spectroscopic observations.

asymmetries, double peaks, multiple absorption components, etc.) that suggest phenomena related to a residual circumstellar accretion disk. The latter group might eventually be classified according to the more detailed classification scheme introduced by Reipurth et al. (1996) for CTTS.

In addition to the Hα line profile types mentioned above, there are four stars that show a complex Hα line profile, characterized by a deep absorption (extending below the continuum) overimposed to a broad emission line. These line profiles are indicated as type 5 in Table 1. All these stars show very broad line profiles indicating rotation rates larger than 80 km s^{-1}, but we cannot rule out that some of them are unresolved multiple spectroscopic systems.

Practically the same conclusions as in Covino et al. (1997) are reached, namely, that stars with Hα filled-in or in absorption dominate among earlier spectral types, while stars with chromospheric Hα clearly dominate among later types and that complex Hα emission is more common among stars of intermediate to late spectral type. This behaviour mainly reflects the dependence of stellar continuum and photospheric Hα absorption on spectral type.

4.2. Lithium equivalent widths

The FOCES and CASPEC spectra were normalized to the continuum level by fitting a spline function using the regions of the continuum spectrum free from absorption and/or emission lines. The lithium equivalent widths have been obtained from the normalized FOCES and CASPEC spectra by integration of the absorption line, interpolating linearly the continuum on both sides of the line. The main source of error in these measurements comes from the uncertainty in the continuum placement. For each spectrum, at least three individual measurements of W(Li) were made by setting the continuum at different positions. The mean estimated error is 10 mÅ in most cases. Only in a few cases of late–type spectra and low S/N, the uncertainty may be as high as 30 mÅ. The lithium equivalent widths W$_{hr}$(Li) for our sample are reported in Table 1.

Problems of line blending and photospheric continuum placement due to rotation, may become important for $v \sin i$ larger than 70 km s^{-1}. Such fast rotators are not common in our sample and they are mostly found among earlier spectral types.

Of the 88 stars observed with FOCES and CASPEC, 26 are spectroscopic binaries or suspected multiple systems (see Sect. 5.1 below). For such stars, the measured line equivalent widths do not correspond to those of the individual stars because the observed photospheric continuum is the total contribution from both components. In addition, two stars (RXJ 0526.5+1510 and RXJ 0543.5−0642) have low S/N FOCES spectra which are not useful for lithium measurements, yet they are suitable for the cross-correlation analysis. Therefore, in the following analysis of the lithium line, we will refer to the restricted sample of the 60 presumably single stars.

By comparison of the low (W$_{lr}$(Li) reported in Paper I) and high-resolution (W$_{hr}$(Li)) lithium equivalent widths, we find, as expected, a general trend to overestimate the W$_{lr}$(Li) values, obviously because of the blend of the lithium line with the nearby Fe lines. The blend is more pronounced for stars earlier than about K6, where the strength of the FeI lines starts to increase (Covino et al. 1997).

Interestingly, for several stars, the W$_{lr}$(Li) values match well with those obtained from high-resolution spectra and, in some cases, for M-type stars, the W$_{lr}$(Li) values are underestimated. The mean difference $<$W$_{lr}$(Li) - W$_{hr}$(Li)$>$ is 35 mÅ with a standard deviation of 60 mÅ. Therefore, we estimate that the W$_{lr}$(Li) for these stars are overestimated by no more than about 95 mÅ.

The fact that the lithium strength may be overestimated on low-resolution spectra is one of the arguments used by some authors (Briceño et al. 1997; Favata et al. 1997) to claim that the majority of the RASS lithium-rich stars found in the general direction of star forming regions are not PMS stars but active ZAMS stars. In the high-resolution spectroscopic study by Covino et al. (1997), it is found that the sample of RASS lithium-rich stars in the Chamaeleon SFR may be contaminated by a sample of likely field stars, most of them being Pleiades-like, and that this sample represents less than 40% of the original one. In recent study, based on high-resolution spectroscopy in the Lupus SFR, Wichmann et al. (1999) find a contamination of ZAMS stars of less than 10%, while in the region south of the Taurus-Auriga SFR Neuhäuser et al. (1997b) find a much larger contamination. However, it is difficult to compare the latter results with those in Chamaeleon or Lupus, because the selection of the ROSAT sources for optical follow-up observations were made differently. Using intermediate resolution spectroscopy, Martín & Magazzù (1999) found a higher fraction (≈40%) of ZAMS stars among the sample of the RASS lithium-rich stars in the general direction of the Taurus-Auriga SFR reported by Wichmann et al. (1996). They find that only a minority of the stars in the original Wichmann et al. (1996) sample agree with Martín's WTTS classification, while several others satisfy Martín's PTTS classification. Martín & Magazzù (1999) find that the majority of Wichmann et al. (1996) stars in Taurus really are PMS stars. However, they do not derive radial velocities from their spectra.

In Fig. 2 the Li I (λ6708 Å) equivalent width versus $logT_{eff}$ for the stars in our sample is shown. The stars with radial velocity (RV) in the range from 21 to 30 km s^{-1}, which is the RV range found for some Orion's stars (Hartmann et al. 1986; Walter et al. 1998, but see Sects. 5 and 6), are marked with a "+". The upper envelopes for young open clusters adopted by Martín & Magazzù (1999) and by Preibisch et al. (1998) are represented by the continuous and dotted lines respectively. Twenty six stars[4] out of the 60 plotted in Fig. 2 satisfy the WTTS criterion by Martín (1997). Of these 26 stars, 15 have RV consistent with stars in Orion. No evidence for the PTTS defined by Martín (1997) is found among the stars in our sample.

[4] without counting those in the intersection area between the WTTS region and the young open cluster region.

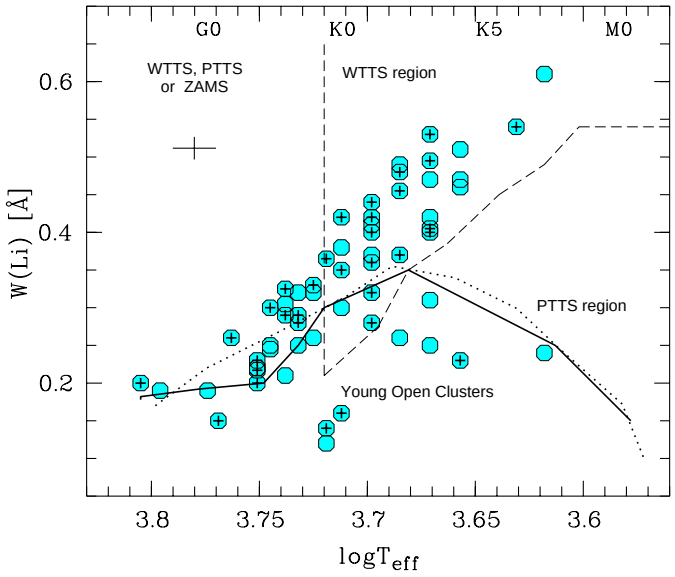

Fig. 2. Lithium equivalent width versus effective temperature for the single stars in the sample (shaded circles). The stars with radial velocity in the range from 21 to 30 km s^{-1} are indicated with a + (see text for details). The mean errors of $logT_{eff}$ and W(Li) are also indicated. The thick and dotted lines represent the upper envelope for young open clusters as adopted by Martín & Magazzù (1999) and Preibisch et al. (1998) respectively, while the dashed line indicates the WTTS and PTTS regions as described by Martín (1997).

Nineteen stars out of the 60 plotted in Fig. 2 fall below or just above the upper envelope of young open clusters adopted by Martín & Magazzù (1999) and 8 of those have RV well consistent with Orion. Therefore, less than 30% of the stars might eventually be contaminating young ZAMS objects. Based on a more conservative classification by Preibisch et al. (1998), who used low-resolution spectra where the lithium equivalent widths may be overestimated, the contamination would be as high as about 35%, mainly due to the G type stars. However, many of these stars are on-cloud objects and have RV consistent with other Orion TTS. Thus, we believe that these are true members of the SFR. Note that the G type stars with a spectrum like RXJ 0540.1-0737 (see Fig. 1), can hardly be classified as ZAMS stars, regardless of their RV. Therefore, WTTS, PTTS and ZAMS stars can be also found in the region occupied by stars earlier than K type. Thus, the upper envelope for stars in young clusters adopted by Martín & Magazzù (1999) seems to be more appropriate for the high-resolution data presented here, and hence, the young ZAMS stars that might eventually contaminate the sample of RASS PMS stars in Orion are expected to be less than 30%.

A careful comparison of the line intensity of Li I λ6708 and of the nearby Ca I λ6718 line in the spectroscopic multiple systems leads to the conclusion that, except for two of them, all the components have lithium stronger than calcium (see examples in Fig. 3) and, hence, are very likely PMS stars (Covino et al. 1999, in preparation).

We have also re-examined the low-resolution spectra of the stars lacking high-resolution in the lithium range and find that most of them (more than 70%) show strong lithium absorption in their low-resolution spectra, typically stronger than the nearby Ca I λ6718 line. These two lines can definitely be resolved in the low-resolution ($\lambda/\Delta\lambda \approx 1800$) spectra.

5. Results

5.1. Spectroscopic binaries

An extremely important byproduct of our high-resolution observations, in combination with cross-correlation analysis, is the discovery of several double-line spectroscopic binaries (SB2's) and higher multiplicity systems among the RASS PMS sample in Orion. Two examples of spectra of PMS SB2, and the corresponding cross-correlation peaks with respect to a standard star of similar spectral type, are shown in Fig. 3.

Among the 106 stars observed with high-resolution, we found 30 stars to be previously unknown spectroscopic binaries (SB's) and suspected multiple systems (see Table 1). In particular, 4 are single-line spectroscopic binaries (SB1's); 3 are double-line spectroscopic binaries[5] for which the two components appear well separated (indicated with SB2 in Table 1, cf. Fig. 3a) in their spectra and by the cross-correlation analysis; other 5 stars also show double lines in their spectra but the two components are almost in blend (indicated with SB2b in Table 1, cf. Fig. 3b); 5 more stars, that show two components in their cross-correlation function, even if not clearly resolved in their spectra because of confusion with noise, can be considered as good candidates for SB2's (indicated as SB2? in Table 1); finally, 4 stars clearly show triple components (ST's) which are resolved spectroscopically (cf. Fig. 3c)[6].

Apart from these 21 confirmed or very likely spectroscopic binaries, there are other 9 stars showing strong asymmetries in their cross correlation peaks that can also be considered as suspected binaries (marked with SB? in Table 1).

In addition, there are other stars for which the RV is suspected to be variable. These stars are marked with VAR? in Table 1. The nature of the RV variations is not clear yet as, in some cases, it might be also related to active regions or to photospheric stellar spots.

To compute the binary fraction in our sample we consider the 12 SB's (SB1 and SB2) plus the 4 ST's out of the 106 targets investigated. Definitions of the binary fraction in the literature vary from author to author, especially when systems of higher multiplicity are included. For the purpose of this paper we define it to be the average number of companions per target studied. The result for our sample is 19%. If we include also the objects that we consider to be good SB candidates (SB2? in Table 1), the

[5] without including the previously known SB2 HBC 447 (Marschall & Mathieu 1998).

[6] For the stars RXJ 0529.4+0041 and RXJ 0539.8−0205 there is a visual companion at about 1.5 arc-sec. Since, typically, a diafragm of 2 arc-sec was used for the FOCES observations, one cannot rule out that the third component in the spectra of these stars is due to a contamination by the visual companion. Whatever the case, the three components show strong Li absorption and hence they are likely to constitute hierarchical triple systems.

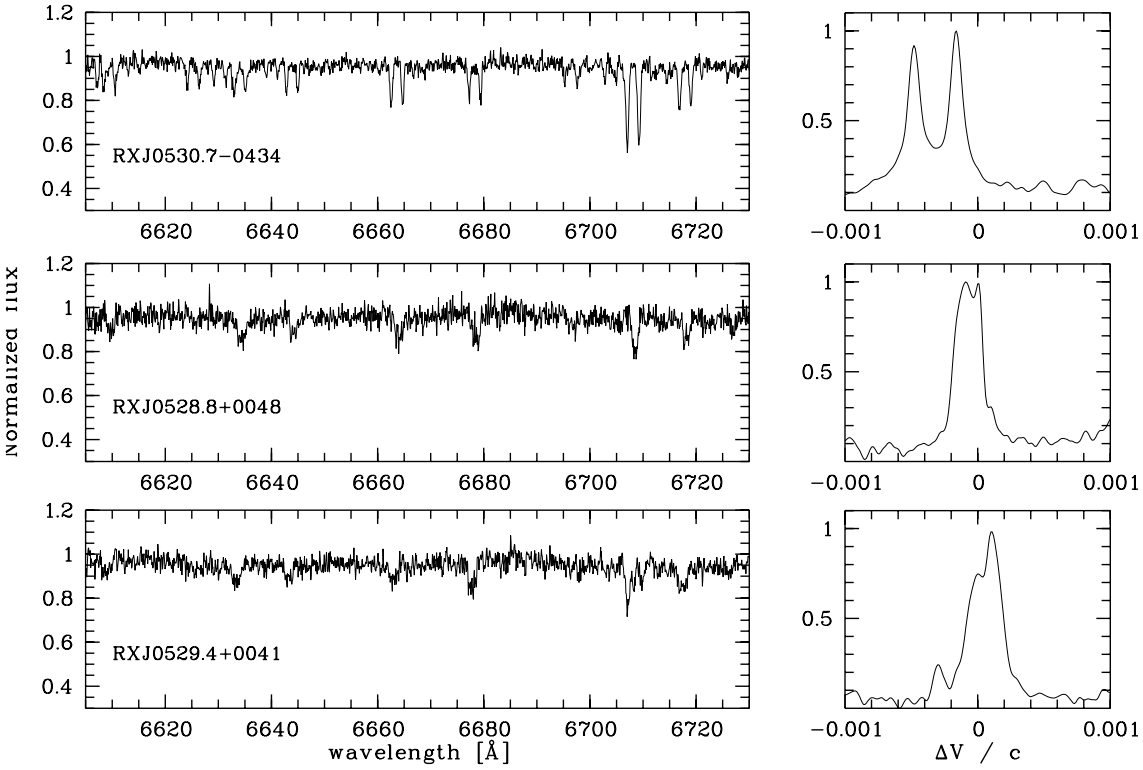

Fig. 3. Examples of spectra of the two spectroscopic binaries RXJ 0530.7−0434 & RXJ 0507.8−0931 (indicated as SB2 and SB2b in Table 1 respectively) and the spectroscopic triple RXJ 0529.4+0041 (indicated as ST3 in Table 1) in the lithium range. Their cross-correlation functions are also shown in the right panels.

binary fraction increases to 24%, which is significantly higher than the value of 10% quoted by Mathieu (1994) for SB's with periods shorter than 100 days. The only caveat here, of course, is that the orbital periods for the stars in our sample are not known. If the more dubious SB's are included (SB?), the excess binary fraction would be even larger.

X-ray selected samples are known to have an enhanced frequency of (generally short-period) binaries because of the increased X-ray activity associated with close pairs, which tends to promote them into the sample where they would otherwise not be included. In the present case this is unlikely to be an important effect because a large fraction of the targets are confirmed to be PMS based on other criteria. Nevertheless, we cannot rule out that a small fraction of our binaries (even if they are PMS) would not have been detected by the RASS had they been single.

For 8 objects visual companions have been found during the spectroscopic observations within less than 10 arcsec from the primary target (see notes in Table 1). This results in a "visual binary frequency" of about 10%, which is probably only a lower limit because of the fact that these companions have not been searched for in any systematic way. In most cases the companions are rather faint and close to their parent stars, and, except for the star RXJ 0539.8-0205 for which there is confirmation of the PMS nature of the visual companion (Covino et al. 1999 in preparation), we do not have spectra to confirm their kinematical (radial-velocity) association to the primaries. However, based simply on the probability of finding other stars at random very close to the primaries, we consider them all likely to be physical companions.

Sterzik et al. (1997) have found a significantly high fraction of visual binaries (3 out of 5) in a sample confined in the λ-Ori region. Though their sample is very small, their finding, in line with ours, can be considered as a hint that the binary fraction in Orion may be unusually high.

For half a dozen of the spectroscopic binaries listed in Table 1, we have collected some repeated observations that are sufficient to allow the determination of the spectroscopic orbit. Double-line spectroscopic binaries are a pre-requisite for determining the masses of the components directly. This is especially important for PMS stars because direct determination of the mass allows to test models of stellar evolution at this very early stage, a regime where the models are essentially unconstrained by the observations so far.

The reason why direct mass determination is so hard to achieve is because, in addition to having a double-line SB, the inclination angle of the orbital plane must be also determined. This usually means that, in order to determine the true masses, the system must also be eclipsing, which is a rare occurrence. Follow-up observations are already in progress to determine whether this is the case for any of the binaries in our sample. In any case, the double-line spectroscopic orbital solutions can at least provide the determination of mass and luminosity *ratios*, as well as lower limits for the masses of the components, which can also serve as constraints on current evolutionary models. A

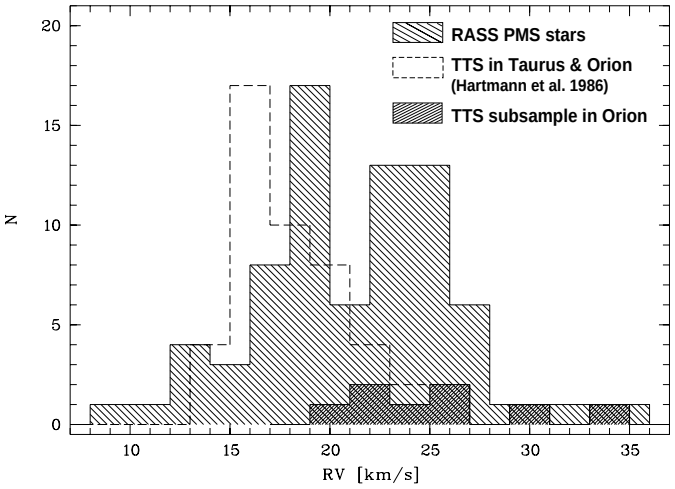

Fig. 4. Radial velocity distribution of the stars observed at high-resolution. The radial velocity distribution of stars in the Taurus–Auriga (dashed histogram) and Orion (cross-hatched histogram) star forming regions by Hartmann et al. (1986) are also shown for comparison.

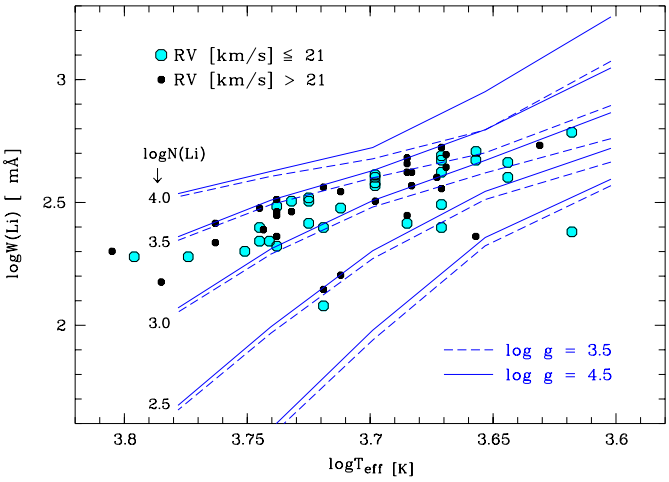

Fig. 5. Logarithm of the lithium equivalent width versus effective temperature for the stars in our sample, in two bins of radial velocity. The iso-abundance curves by Pavlenko and Magazzù (1996) for two surface gravity values are also plotted.

detailed discussion of these issues and the analysis of orbital solutions for the spectroscopic systems currently under investigation is deferred to a forthcoming paper.

5.2. The radial velocity distribution

In Fig. 4 the RV distribution of the RASS stars in Orion (RV_{RASS}) is compared with the RV distribution of T Tauri stars in Taurus and Orion by Hartmann et al. (1986). The spectroscopic multiple systems or suspected SB's are not included in these distributions. The RV_{RASS} distribution is broad with a velocity dispersion of about 10 km s^{-1}.

The velocity range of the RV_{RASS} distribution is a consequence of the fact that the RASS stars are scattered over a large area (and volume) in the direction of Orion. We stress that the RV distribution of the molecular cloud cores in Orion also covers a similar range in RV showing a clear velocity gradient in the Orion A cloud at lower declinations (Maddalena et al. 1996; Tatematsu et al. 1998, see Sect. 6).

The RV_{RASS} distribution apparently shows a double peak suggesting two kinematical groups. The upper limit for the error of 2 km s^{-1} in our RV determinations suggests that the double peak may be real.

A double Gaussian fit to the RV_{RASS} distribution yields peaks at 18.5 and 25 km s^{-1}, with velocity dispersions of 3.0 and 4.5 km s^{-1}, respectively. Assuming an *arbitrary* dividing line at RV≈21 km s^{-1}, which corresponds to the minimum between the two peaks, to define the two hypothetic kinematical groups, it is found (c.f. Sect. 6.1) that objects with RV $>$ 21 km s^{-1} tend to be more correlated, both spatially and kinematically, with the CO emission peaks of the Orion A & B clouds and with the Ori OB1a association, while the others appear more dispersed and distributed throughout the entire studied area (see Sect. 6).

The dividing RV limit of 21 km s^{-1} is arbitrary and, if two kinematical groups do really exist, from our double Gaussian fit we estimate that roughly 1/5 of the total number of stars in each distribution (≈ 7 stars) may contaminate the other. Despite this, the conclusions regarding the spatial distribution (and lithium: see next section) do not change.

Another possibility is that the sample of RASS stars in the general direction of Orion might be a mixture of two groups of young stars: one group consistent with the kinematics of Orion stars, at about 460 pc, while the other group, having RV's more consistent with Taurus might be closer than Orion. However, a possible relationship of the latter group with the Taurus SFR is excluded, as these stars would be projected about 70 pc away from the currently active SFR in Taurus. As we will discuss in Sect. 6, some stars of the second kinematical group might be related instead to the inner rim of the Gould Belt.

5.3. Lithium abundance

In Fig. 5, the logarithm of the lithium equivalent width of the stars observed with high resolution is plotted versus the logarithm of the effective temperature in the two bins of RV, as defined from the radial velocity distribution. We also report in the plot the lithium iso-abundance curves by Pavlenko and Magazzù (1996), for two values of surface gravity. Except for the fact that there seems to exist a trend (which is not statistically significant) for the stars with RV $>$ 21 km s^{-1} to have more Li, there is no difference in lithium abundance between the two RV groups.

A spread in the lithium strength is observed at each spectral type probably due to the fact that, at each spectral type, we have stars of different age and/or different rotation rates (see Sect. 5.4)[7]. Note, however, that regardless of their RV, most of the stars in the sample have $logN(Li)$ values between 3.0 and

[7] Rotational modulation of the Li line due to a spotted photosphere (see Fernández & Miranda 1998 and Neuhäuser et al. 1998) may also contribute to the spread.

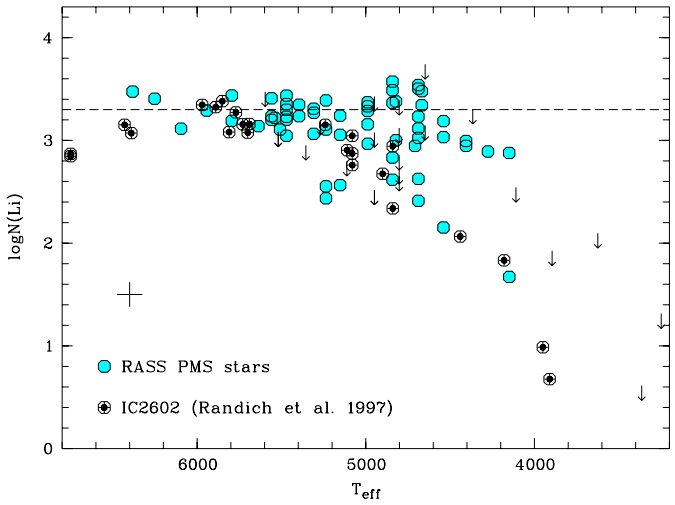

Fig. 6. Lithium abundance versus effective temperature for the stars in our sample. Stars lacking high-resolution spectroscopy are represented by upper limits. The stars of the young cluster IC 2602 by Randich et al. (1997) are also plotted. The dashed line represents the cosmic lithium abundance of 3.3 in the $log(H) = 12$ scale.

3.5 and only a few have $logN(Li)$ less than 2.5. Hence, most of the stars in the sample have lithium abundance consistent with low mass PMS stars and, as it will be shown in Sect. 6, the fact that some of them have RV $<$ 21 km s^{-1} does not necessarily mean that these stars are not associated with the Orion SFR.

We have derived lithium abundances in the $log(H) = 12$ scale, from the W(Li) and T_{eff} values and using the non-LTE curves of growth reported by Pavlenko & Magazzù (1996), assuming $log\ g$=4.5. The lithium abundances derived in this way are reported in Table 1. The main source of error in the derived $logN(Li)$ values is the uncertainty in the effective temperature. The estimated mean uncertainties on T_{eff} are on the order of ΔT_{eff} ≈150 K. Taking this and a mean error of about 15 mÅ in W(Li) into account, we estimate a mean error on the order of 0.15 to 0.2 dex in $logN(Li)$. However, the assumption of $log\ g$=4.5 may affect significantly the lithium abundance determination (cf. Fig. 5), in the sense that a lower surface gravity yields a higher lithium abundance. In particular, for stars with $\log T_{eff}$ less than about 3.7 (≈ 5000 K) and $\log W(Li)$ greater than about 2.5 (≈ 320 mÅ), the difference in $\log N(Li)$ may rise to 0.3 dex, when assuming $\log g$ of 3.5. Hence, assuming $\log g = 3.5$ would result in higher lithium abundances than when assuming $\log g = 4.5$. Thus we adopt, as a more conservative assumption, $\log g$=4.5 but keep in mind that the abundances derived for the stars with high-resolution spectroscopy may eventually be underestimated.

We have also derived lithium abundances for the stars without high-resolution spectroscopy in the same way, but using the W$_{lr}$(Li) values reported in Paper I. However, although we also assume $log\ g$=4.5, these abundances may be regarded as upper limits because of the likely overestimation of the W$_{lr}$(Li) values from low-resolution spectra.

In Fig. 6 we show the $\log N(Li)$ versus T_{eff} relation for the stars with high resolution spectroscopy[8]. The stars lacking high-resolution are plotted as upper limits. For comparison, we also plot the stars of the young cluster IC 2602 reported by Randich et al. (1997), for which the lithium abundance was re-determined by us in a consistent way (i.e. using the same temperature scale and curves of growth as for the RASS stars).

Only three of the RASS stars fall below the values derived for IC 2602. Furthermore, as discussed above, the Lithium abundances may be underestimated for some stars, because of the $log\ g$=4.5 assumption. Therefore, most of these stars should be as young as, or younger than the IC 2602 stars. Again, a vertical spread in $\log N(Li)$ at a given spectral type can be seen, probably reflecting a spread in age and/or in the rotation rates of these stars (see Sect. 5.4). Another reason of the spread in $\log N(Li)$ is due to errors in the assumed gravity, as discussed above, and to the uncertainty in the effective temperature.

5.4. Rotation versus Lithium

A large spread in the rotation rates may introduce a spread in the lithium abundance at each mass bin, as found for stars in α Per (Balachandran et al. 1988) and in the Pleiades (Soderblom et al. 1993). Stars in the PMS phase, however, have not yet suffered sufficient Li depletion for such a trend to be observed. On the other hand, the Li burning might be inhibited in the PMS stellar evolution: it has been suggested that fast rotation might reduce the process of Li depletion (Martín & Claret 1996). However, the latter result is in contrast with the results by Pinsonneault et al. (1990) and more recent results by Sanctos Mendes et al. (1997) who find that rotating models deplete more lithium than non-rotating models. Lithium burning might be linked to the dynamo induced magnetic fields at the base of the convective layers due to rotation (D'Antona & Mazzitelli 1997; Ventura et al. 1998).

We point out that, in our sample, the stars later than about K0 which fall just below the upper envelope for young open clusters have $v \sin i <$ 20 km s^{-1} and, hence, their relatively high lithium cannot be ascribed to rapid rotation and/or induced dynamo effects. We also stress that about half of the stars falling in the young open clusters area have RV's consistent with Orion's stars (cf. Fig. 2) and practically all of them have $v \sin i <$ 20 km s^{-1}.

The $logN(Li)$-$v \sin i$ relation is shown in Fig. 7. While the stars with $v \sin i$ greater than about 50 km s^{-1} (practically all earlier than K0) show a dispersion of about 0.25 dex in $logN(Li)$, the stars with $v \sin i$ less than about 50 km s^{-1} (typically later than about K0) show a dispersion of more than 1 dex in $logN(Li)$. This mainly reflects the mass dependence of Li depletion: slow rotators, which dominate among lower mass stars, seem to show a larger dispersion in $logN(Li)$ while, faster rotators, typically higher mass stars, show a lower dispersion in $logN(Li)$.

[8] For the sake of clarity and since there is no difference in the lithium strength of stars with different RV, here we do not divide the sample into the two bins of RV described above.

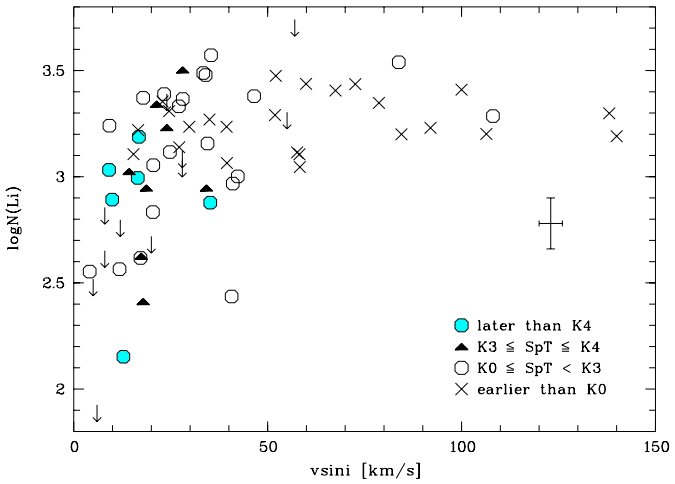

Fig. 7. $logN(Li)$ versus $v \sin i$ relation for the stars in our sample. The different symbols represent different intervals of spectral type. The stars with spectral type later than K0 that lack high-resolution spectroscopy in the lithium range are represented as upper limits.

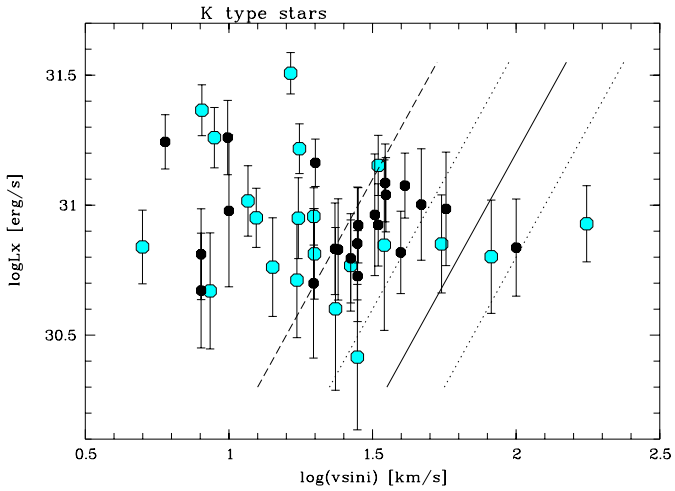

Fig. 8. Scatter plot of $logL_X$ versus $log(v \sin i)$ for the K type stars. The black dots represent stars with radial velocities larger than 21 km s^{-1}, while the shaded circles represent those with radial velocities $\leq$ 21 km s^{-1}. The continuous line is the relation $logL_X = 2 \cdot logV_{rot} + 27.2$ from Bouvier (1990). The two dotted lines represent the upper and lower envelopes for late type dwarfs and dKe-dMe stars, while the dashed line represents the upper envelope for the T Tauri stars from Bouvier (1990).

Regardless of the radial velocity bin, stars with spectral types in the range from G2 to K4 show a trend similar to the one observed in the Pleiades, ie. a larger vertical spread for slower rotators than for more rapidly rotating stars. The latter are more frequent among earlier spectral types. Such a trend disappears completely if the stars below the Pleiades envelope are not considered. Thus, the observation of some dispersion in the lithium strength for the slow rotators may be attributed to the fact that the late type stars might be a mixed population of PMS stars and low lithium late type stars with W(Li) $<$ 200 mÅ. Therefore, although an apparently larger dispersion in the lithium strength is observed for the stars with $v \sin i <$ 20 km s^{-1} than for the stars with $v \sin i >$ 20 km s^{-1}, the trend is not so clear as for young main sequence stars. This result is also in line with the findings by Duncan & Rebull (1996) for a sample of stars in the Orion nebula region.

5.5. Rotation versus X-ray emission

Of particular interest is the analysis of the rotation–activity connection in homogeneous samples of active stars. We have derived X-ray luminosities for the stars in our sample in the same way as described in Sect. 4.6 of Alcalá et al. (1997), but assuming a distance of 460 pc for all the stars. The resulting X-ray luminosities are listed in Table 1.

We do not see a clear correlation between the X-ray luminosity (derived from RASS observations) and $v \sin i$ in our sample. However, because of the dependence of $v \sin i$ on the mass, we restrict our sample to a range of spectral type. In Fig. 8 the $logL_X$ versus $log(v \sin i)$ relation is shown for the K type stars. The different symbols indicate the two RV bins defined in Sect. 5.2. Only stars for which no evidence of binarity is found are shown in the plot.

The continuous line in Fig. 8 represents the relation $logL_X = 2 \cdot logV_{rot} + 27.2$ for dwarfs derived by Bouvier (1990); the "right" and "left" envelopes for dwarfs and dKe-dMe stars, estimated by eye from Fig. 1 of Bouvier (1990), are also shown as dotted lines; finally, the "left" envelope for the T Tauri stars studied by Bouvier (1990) is represented as a dashed line.

Except for the star RXJ 0551.2-0653[9], all other stars fall well to the left side of the $logL_X - logV_{rot}$ relation, as expected, since the $v \sin i$ values must be considered as lower limits for the stellar rotational velocity.

Note that 17 of the 23 stars with RV $>$ 21 km s^{-1} fall in the area defined by the T Tauri stars studied by Bouvier (1990), while only 7 of the 22 stars with RV $\leq$ 21 km s^{-1}, fall in that area. Therefore, despite the large errors in the X-ray luminosity and the fact that the $v \sin i$ values are only lower limits of the stellar rotational velocity, the majority (74%) of the stars with RV $>$ 21 km s^{-1} seem to be more consistent with the rotation–coronal activity relation for the T Tauri stars studied by Bouvier (1990), unlike the stars with RV $\leq$ 21 km s^{-1}. The latter tend to be more scattered towards higher X-ray luminosities and lower $v \sin i$ values. There are two effects that may produce this scatter: the dispersion towards lower $v \sin i$ values, most likely due to the projection effect, and the vertical dispersion, that might be due to a systematic overestimate of the X-ray luminosities caused by an overestimation of the distance. The combination of these two effects will shift the points towards the upper-left corner of the $logL_X$ versus $log(v \sin i)$ plane. This would be consistent with the fact that, if a dynamo mechanism is in operation, slow rotators, with a low level of coronal activity, will be

[9] Only one CfA spectrum is available for this star, and hence its RV and $v \sin i$ determinations are rather uncertain. Also we cannot exclude that RXJ 0551.2-0653 is an unresolved SB for which the $v \sin i$ value is overestimated

more easily detected by the flux-limited RASS if they are closer than 460 pc.

Another cause for the "overestimation" of the X-ray luminosity are possible long-period SB stars undetected by the high-resolution spectroscopy due to their long orbital periods and small relative radial velocity variations, spatially unresolved.

6. Discussion

The identification of a significant number of low-mass PMS stars in the general direction of SFR's on the basis of the RASS has been disputed by some authors (Briceño et al. 1997; Favata et al. 1997; 1998), who claim that the vast majority of the RASS lithium-rich stars in SFR's must be mainly active ZAMS stars. One of the main arguments of these authors is the fact that the strength of the lithium line was overestimated in the low-resolution spectra of the identified RASS stars. However, for the particular case of Orion, Briceño et al. (1997) claim that the sample reported in Paper I may be biased toward truly young stars.

In the present high-resolution spectroscopic study, we have found that the youth of the RASS stars in the general direction of Orion reported in Paper I, is well supported by the strong lithium absorption line compared with that of ZAMS stars in young open clusters of the same spectral type. Moreover, their lithium abundance is comparable to that of well known low-mass PMS stars. Hence, unless current ideas on lithium depletion are completely wrong, these stars must be low-mass PMS stars.

In addition to the findings reported in this paper, other recent studies conducted with high-resolution spectroscopy (Covino et al. 1997; Wichmann et al. 1999) have confirmed the PMS nature of the RASS lithium-rich stars. Moreover, Neuhäuser & Brandner (1998) have found that all the lithium-rich ROSAT counterparts having Hipparcos parallaxes fall indeed well above the ZAMS. Therefore, it is not our intention in this paper to discuss the reasons why the models that claim the RASS lithium-rich stars in SFR's to be mainly active ZAMS stars are inconsistent with the observations. The interested reader is referred to the relevant sections by Covino et al. (1997) and Wichmann et al. (1999) in which the latter arguments are discussed.

Here we discuss the spatial distribution of the RASS PMS stars in the general direction of Orion, their association with the Orion clouds and the possibility of the association of some of them with the Gould Belt.

6.1. Spatial distribution versus radial velocity

The Orion SFR contains several clouds and filamentary cloud structures which show up in the CO molecular emission maps (Maddalena et al. 1986; Tatematsu et al. 1998) as well as in the IRAS 100 μm maps. Such structures extend over an area even larger than the one investigated on the basis of RASS data. Therefore, one should expect that the star formation process in Orion took place in a large volume, in different parts of the complex. In fact, the Kiso objective prism survey in Orion (Wiramihardja et al. 1989; 1991; 1993; Kogure et al. 1989) detected 1157 on and off cloud Hα emission line objects down to V=17.5 and distributed over 150 deg^2 from 5^h9^m to 5^h51^m in right ascension and from -13° to +2°48' in declination. Kogure et al. (1992) followed-up, with low-dispersion spectroscopic observations, 34 emission line stars in Ori OB1b, and concluded that they were indeed T Tauri stars based on H-Balmer and CaII K emission lines. Nakano and McGregor (1995) obtained near-IR photometry for a number of these stars, and also concluded that they were mostly T Tauri stars. Many of the Kiso objects, as the RASS PMS stars, are found far off the Orion molecular clouds. More recently, Dolan & Mathieu (1999) performed a lithium survey around λ Ori and found 72 lithium rich objects with RV consistent with Orion. Therefore, it is not surprising to find X-ray emitting PMS stars distributed in the whole Orion complex. Furthermore, there is a good spatial correlation between the RASS sources in Orion and the Kiso Hα emission line objects (see Walter et al. 1999).

The spatial distribution of the stars reported in Paper I shows that the ROSAT on–cloud PMS stars, on the A and B clouds, as well as on the fragments of the λ Ori region and those located in the Ori OB1a association, are more clustered than the off-cloud PMS stars. Most of the ROSAT off–cloud PMS stars are located south-west of the A cloud. It has been shown in Paper II that the stars with the highest lithium excess δW(Li) relative to the upper envelope for the Pleiades tend to concentrate toward the molecular clouds. On the basis of the high-resolution spectroscopy, we confirm the latter result. However, there are also many other stars in the sample with lithium excess that are found far off the Orion molecular clouds, and where Kiso Hα emission line objects are also found.

As mentioned in Sect. 5.2, the RV distribution of the single stars in our sample suggests two kinematical groups, but the fact that some stars have RV < 21 km s^{-1} does not necessarily mean that they are not associated to the Orion complex: the velocity distribution of the clumps studied by Maddalena et al. (1986) in the whole Orion complex is peaked at a *local standard of rest* (LSR) velocity of about 10 km s^{-1}, but the distribution spans from about 0 to about 16 km s^{-1}. Therefore, in order to investigate in more detail the radial velocity of the RASS stars in relation with their spatial distribution and their possible association with the molecular cloud cores, we have transformed the heliocentric RV's of the RASS PMS stars to the LSR.

In Fig. 9 the velocity distribution of the CO emission peaks by Maddalena et al. (1986) (thick line) is compared with the LSR velocity distribution of the RASS PMS stars (dashed line and hatched histograms). Though a small shift toward more negative velocities is apparent in the distribution of the stars relative to that of the CO emission peaks, the velocity range of the two distributions are similar. The two peaks of the distribution of the RASS PMS stars appear again and become more pronounced when the stars with $\delta W_{hr}(\mathrm{Li}) > 0$ are selected (cross-hatched histogram)[10]. One of the peaks of this distribution clearly coin-

[10] Note that stars with $\delta W_{hr}(\mathrm{Li}) < 0$ also have RV consistent with the CO emission peaks

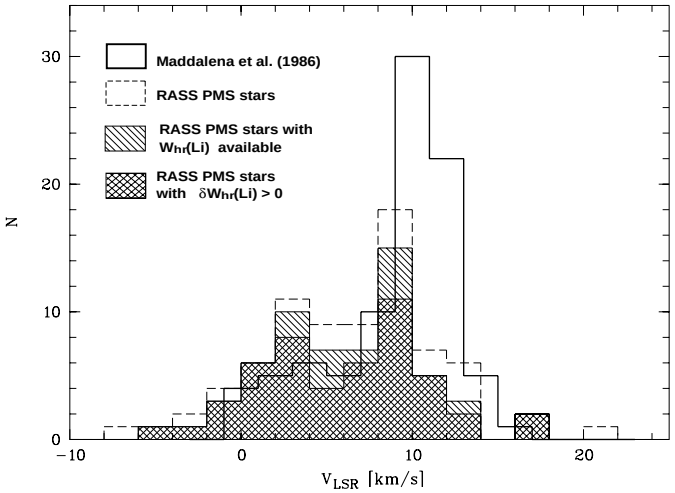

Fig. 9. LSR velocity distribution of the RASS PMS stars (hatched histograms). The LSR velocity distribution of the CO emission peaks from Maddalena et al. (1986) (thick line) is also overplotted.

cides, within the errors, with the peak at about 10 km s^{-1} of the CO velocity distribution. The other peak of the distribution still falls in the range of the CO emission peaks. Therefore, it is important to check whether there is a spatial correlation between the RASS PMS stars and CO emission peaks with similar LSR velocities.

In Fig. 10 we show the spatial distribution of the RASS PMS stars (filled symbols) in four bins of LSR velocity. For sake of clarity, we represent the four velocity bins in four different panels (Figs. 10a,b,c & d). For comparison, on each panel the spatial distribution of the CO emission peaks from Maddalena et al. (1986) is also shown (with the corresponding open symbols), in the same LSR velocity bin. The RASS PMS stars with δW$_{hr}$(Li) less than the conservative value of 20 mÅ (see Covino et al. 1997 & Wichmann et al. 1999) are marked with a cross. We observe the following:

– Although the RASS PMS stars are dispersed over the SFR, there is a general trend for stars in a given RV bin to be located in the same areas as the CO emission peaks with similar LSR velocities. The most dispersed stars with respect to the CO emission (both spatially and in velocity) are those with LSR velocities less than 2 km s^{-1} located to the south-west of the A-cloud (cf. Fig. 10a).
– The clustering of the RASS PMS stars seems to increase with velocity, ie. the RASS PMS stars with smaller radial velocities (cf. Fig. 10a) tend to be gradually more scattered than those with higher velocities (cf. Fig. 10d): most (85%) of the stars with LSR velocities greater than 6 km s^{-1} (Figs. 10c & d) are on-cloud objects or are found on the λ Ori region, while only 60% of the stars with LSR velocities below 6 km s^{-1} are located on the λ Ori region or are on-cloud objects. Eleven stars with LSR velocities less than 6 km s^{-1} are found spread to the south-west of the A-cloud (cf. Figs. 10a & 10b) and to the right of the dashed line.
– Among the RASS PMS stars with LSR velocities greater than 6 km s^{-1} (Figs. 10c &d) located on the A & B clouds, those with LSR velocity in the range from 6 to 10 km s^{-1} seem to prevail at lower declinations, while the RASS PMS stars with LSR velocity greater than 10 km s^{-1} tend to lie at declinations larger than about -4 degrees. Therefore, the RASS PMS stars located on the Orion A & B clouds apparently show a velocity gradient with declination, which is consistent with the velocity gradient from South-East to North-West in the Orion A-cloud, revealed by the CO emission map reported by Maddalena et al. (1986), and by the CS emission observed more recently by Tatematsu et al. (1998).

We stress that the RV distribution of field stars (as found from RV catalogs) in the area studied with the RASS in Orion, is much flatter than the RV distributions shown in Figs. 4 and 9 and spans from about -150 km s^{-1} to about +100 km s^{-1}. This is strengthened by the results of the unbiased lithium surveys conducted by Walter et al. (1998) in the one degree field around σ Ori and by Dolan and Mathieu (1999) around λ Orionis. Walter et al. (1998) show that the RV distribution of a randomly-selected sample of stars near σ Orionis is significantly different from the RV distribution of the low-mass PMS stars, which, on the other hand, is peaked at about 25 km s^{-1} and spans from +10 km s^{-1} to +40 km s^{-1}. The latter is quite consistent to the velocity distribution of the RASS PMS stars.

Therefore, the RASS low-mass PMS stars with LSR velocities greater than 6 km s^{-1} (RV$\approx$21 km s^{-1}) correlate with the CO emission peaks, both spatially and kinematically. This is a further confirmation of their association with the Orion complex.

Among the stars with LSR velocities less than 6 km s^{-1}, the most dispersed in the sample are those with LSR velocities less than 2 km s^{-1}. However, except for their peculiar spatial distribution and low velocities, all other properties, in particular their lithium abundance, are indistinguishable from those of the other RASS PMS stars. The lithium excess δW$_{hr}$(Li) of these stars is higher than 20 mÅ and, except for RXJ0500.4-1054, their $logN(Li)$ values are larger than 3.1. The present location of these stars with respect to the main Orion clouds is hard to explain in terms of a slow isotropic drift from their parent clouds with a velocity dispersion of 1-2 km s^{-1}, as found in T associations. Therefore, it is likely that the remnant cloud material from which they were formed has already been dispersed (Feigelson 1996). Mizuno et al. (1998) carried out a high sensitivity CO survey over a large area in the general direction of the Chamaeleon SFR. They detected 25 dense cloudlets widely distributed in the areas where RASS PMS stars are found. Therefore, at least for the case of the Chamaeleon SFR, the cloudlet scenario seems to be consistent with the observations. Some of the seemingly off-cloud PMS stars may have been ejected from the star forming cloud cores, as suggested by recent ejection models (Sterzik & Durisen 1995; Kroupa 1998).

Another possibility is that some of the more dispersed RASS PMS stars with LSR velocities less than 6 km s^{-1} are associated

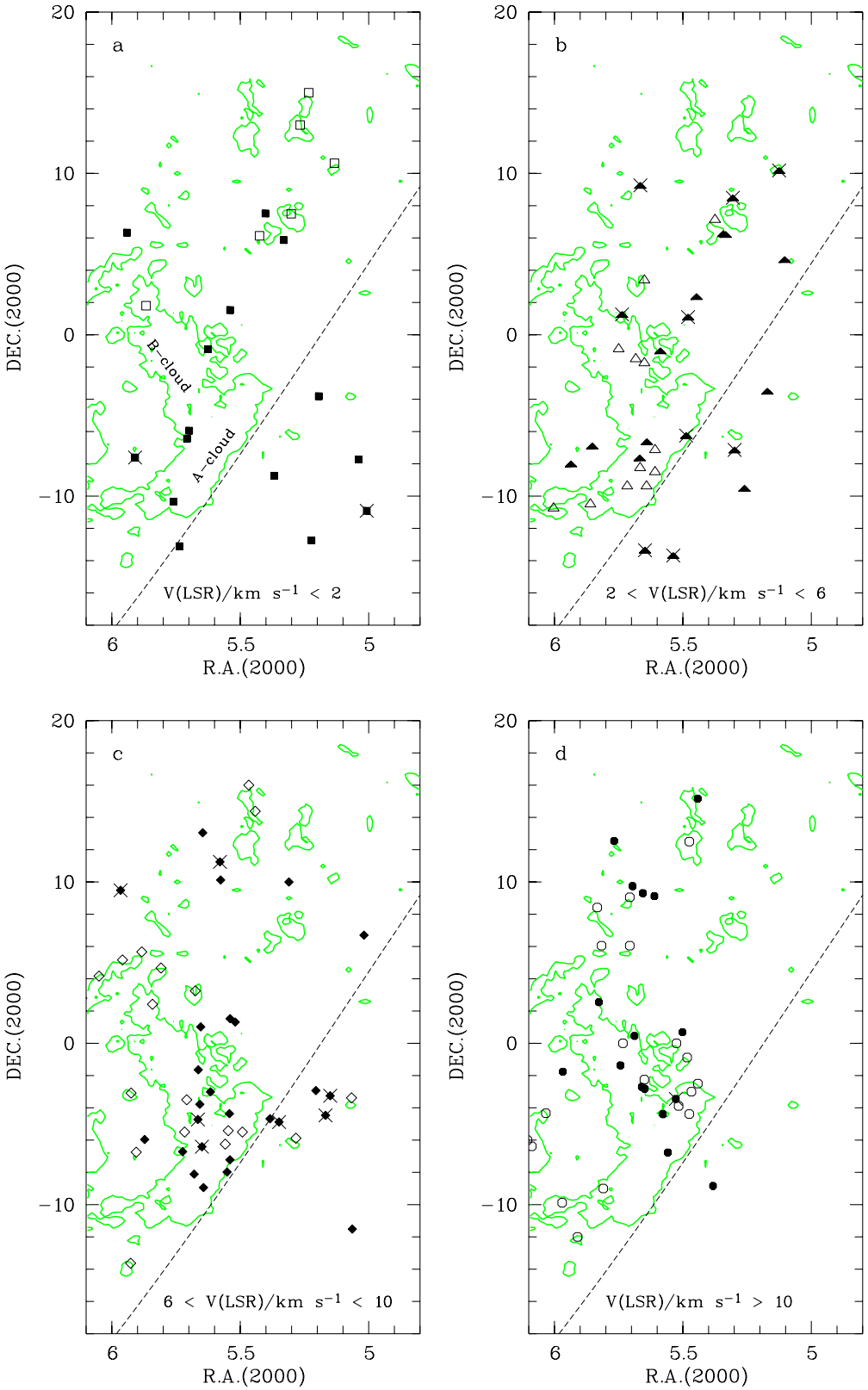

Fig. 10a–d. Spatial distribution of the RASS PMS stars (filled symbols) in Orion in four bins of LSR velocity (different symbols represent the different LSR velocity bins). The stars falling below or just above the upper envelope of young open clusters (cf. Fig. 2) are marked with a "×". The spatial distribution of the CO emission peaks from Maddalena et al. (1986) in the same LSR velocity bins are also overplotted (open symbols). The outlines of the CO line radio-survey by Maddalena et al. (1986) are overplotted as a shaded line in each panel. The dashed line indicates the mean position of the Gould Belt.

with the Gould Belt. The analysis of the spatial distribution of RASS sources, in an area of more than 5000 square degrees in the general direction of Orion, reveals a large-scale structure that crosses the field in a ≈ 20 deg broad lane, located about 15 deg south of the galactic plane (Sterzik et al. 1998, Walter et al. 1999). This structure generally coincides with the Gould Belt in that direction of the sky.

From the correlation between RASS sources and the Tycho catalogue, Guillout et al. (1998) found that the inner rim of the Gould Belt, for the specific direction of Orion, appears to be located beyond 300 pc from the Sun. Assuming an X-ray flux limit of 0.03 counts s^{-1} implies that the RASS could detect PMS stars with X-ray luminosities above $10^{30.5}$ erg s^{-1}, i.e. the high X-ray luminosity tail of the X-ray luminosity distribution function. Actually, the X-ray luminosities reported in Table 1 are consistent with that value.

When observing in the general direction of Orion, three times more distant than other well known SFRs like Taurus, Chamaeleon or Lupus, we are actually looking through a larger space volume along the line of sight. The apparent gradual clustering of the stars with LSR velocities higher than 6 km s^{-1} might be due to a projection effect: the more consistent the LSR velocity of a star with the LSR, the closer the star to the LSR. Therefore, the stars with absolute LSR velocities near zero may appear more spread because they are closer to us than those with LSR velocities greater than 6 km s^{-1}.

On the other hand, Hipparcos data indicate that the Orion OB1a association might be located at 330 pc (Brown et al. 1998). Given the extension of the Orion complex, we cannot rule out that some PMS stars found in that direction, in particular those found in flux limited X-ray surveys, are closer than other Orion members at 460 pc. Therefore, it is very difficult to distinguish the dispersed Orion PMS stars from Gould Belt objects. In particular, the eleven stars with LSR velocities less than 6 km s^{-1}, seen to the right of the dashed line in Figs. 10a and 10b, are good Gould Belt candidate members.

We investigated if there is a difference between the magnitude and lithium distributions of these stars relative to the other stars. Except for the fact that there is a weak trend, not statistically significant, for such stars to be brighter than the others, we do not find any difference. However, the resulting samples are too small to reveal statistically significant differences. Hence, we cannot rule out that these stars are closer than 460 pc and that are Gould Belt members.

The data sample and the area surveyed here are still too small to reveal differences in the observables of the stars, making the trends not statistically significant. The study of large samples of PMS stars distributed on a larger scale than the one studied here and the comparison of their properties with those of the Orion PMS stars, will help to elucidate the topics regarding the formation of low-mass stars on a large scale and their association with the Gould Belt. However, in order to determine the structure of the Gould Belt we have to wait for future satellite missions, like the GAIA project, which will provide accurate parallaxes for large samples of stars towards the general direction of SFRs.

7. Summary and conclusions

We have studied with high-resolution spectroscopy the sample of RASS lithium-rich stars found dispersed in the Orion SFR. From the high-resolution spectroscopy we have derived radial and projected rotational velocities as well as effective temperatures for the stars in the sample. The comparison of the lithium strength of these stars with that of ZAMS stars in young open clusters of the same spectral type shows that the possible contamination of our sample by active disk ZAMS stars is less than 30%. Several double line spectroscopic binaries and multiple systems were found. There are indications that the fraction of spectroscopic binaries in Orion may be significantly higher than in other SFRs. However, this might be also consequence of an observational bias due to the fact that close binaries are more likely to be detected in X-rays than single stars.

The radial velocity distribution, in the LSR, of the RASS PMS in Orion spans from about -2 km s^{-1} to about $+15$ km s^{-1} which is consistent with the range observed for the CO emission peaks in Orion by Maddalena et al. (1996) and with the RV distribution of low-mass PMS stars found recently in unbiased lithium surveys. All these RV distributions are significantly different from that of field stars towards Orion.

The spread in the lithium abundance induced by rotation, as observed for stars in clusters like α Per or the Pleiades, is not evident in the stars in our sample. However, it is not clear whether some of the spread is due to the fact that we are dealing with a mixed population. Part of the spread may be attributed to the uncertainty in the surface gravity of the stars.

The X-ray emission versus $v \sin i$ relation for the RASS PMS stars in our sample does not contradict the relation observed for the T Tauri stars in Taurus. No correlation between X-ray emission and lithium content is observed in our sample.

Finally, we find that at least 60% of the RASS PMS in Orion are well correlated, both spatially and kinematically, with the Orion molecular clouds. Therefore, they can be associated with the Orion molecular complex. The cloudlet scenario seems to be the most reliable explanation for the other more dispersed PMS stars found with the RASS in SFRs but, we cannot rule out that some of the RASS PMS towards Orion, in particular those found more dispersed in the region with LSR velocities of less than about 6 km s^{-1}, might be closer than Orion and be members of the Gould Belt.

Acknowledgements. We thank the referees Drs. G. Basri and E. Martín for their constructive criticism and suggestions which helped to improve the paper. We are grateful to Prof. T. Gehren for providing us with some of the routines for the FOCES data reduction and to Prof. G. Smaldone for his advice on implementing additional IDL routines. We thank the Calar Alto staff, in particular F. Hoyo, M. Alises and A. Aguirre for their technical support during the observations. The technical support by E. Matamoros and A. Sánchez at the ESO 3.6 m telescope is also acknowledged. We also thank the observers at the CfA telescopes, P. Berlind, M. Calkins, J. Caruso, R. Davis, E. Horine, D. Latham, A. Milone, J. Peters, R. Stefanik, and J. Zajac for their usual proficiency, and R. Davis for maintaining the CfA database of radial velocities. ROSAT is supported by the German government (BMBF/DLR) and the Max-Planck-Society. RN wishes to acknowledge financial support

from the DFG Star Formation program. This work has been supported in part by a grant from the Italian Ministery of University and Scientific and Technological Research.

References

Alcalá J.M., Krautter J., Schmitt J.H.M.M., et al., 1995, A&AS 114, 109
Alcalá J.M., Terranegra L., Wichmann R., et al., 1996, A&AS 119, 7 (Paper I)
Alcalá J.M., Krautter J., Covino E., et al., 1997, A&A 319, 184
Alcalá J.M., Chavarría-K. C., Terranegra L., 1998, A&A 330, 1017 (Paper II)
Balachandran S., Lambert D.L., Stauffer J.R. 1988, ApJ 333, 267
Bouvier J., 1990, AJ 99 946
Bouvier J., Wichmann R., Grankin K., et al., 1997, A&A 318, 495
Briceño C., Hartmann L.W., Stauffer J.R., et al., 1997 AJ 113, 740
Brown A.G.A., Walter F.M., Blaauw A., 1998, In: Burkert A., McCaughrean M. (eds.) The Orion Complex Revisited. Proceedings of the 1997 Rinbgberg Conference on Orion., PASP conf. Ser. in press
Covino E., Alcalá J.M., Allain S., et al., 1997, A&A 328, 187
D'Antona F., Mazzitelli I., 1994, ApJS 90, 467
D'Antona F., Mazzitelli I., 1997, Mem. Soc. Astron. Ital. vol. 68, p. 807
de Jager C., Nieuwenhuijzen H., 1987, A&A 177, 217
Dolan C.J., Mathieu R.D, 1999, AJ, in press
Duncan D.K., Rebull L., 1996, PASP 108, 738
Favata F., Micela G., Sciortino S., 1997, A&A 326, 647
Favata F., Micela G., Sciortino S., D'Antona F., 1998, A&A 335, 218
Feigelson J.D., 1996, ApJ 468, 306
Feigelson E.D., Kriss G.A., 1989, ApJ 338, 262
Fernández M., Miranda L.F., 1998, A&A 332, 629
Ghorti U., Batt H.C., 1996, MNRAS 278, 611
Gray D.F., 1976, The observation and analysis of stellar photospheres. Wiley & Sons Inc., 394
Guillout P., Sterzik M.F., Schmitt J.H.M.M., Motch C., Neuhäuser R., 1998, A&A 337, 113
Hartmann L.W., Hewett R., Stahler S., Mathieu R.D., 1986, ApJ 309, 275
Kogure T., Yoshida S., Wiramihardja S.D., et al., 1989, PASJ 41, 1195
Kogure T., Ogura K., Nakano M., Yoshida, S., 1992, PASJ 44, 91
Krautter J., Alcalá J.M., Wichmann R., Neuhäuser R., Schmitt J.H.M.M., 1994, Rev. Mex. Astron. Astrofis. 29, 41
Krautter J., Wichmann R., Schmitt J.H.M.M., et al., 1997, A&AS 123, 329
Kurtz M.J., Mink D.J., 1998, PASP 110, 934
Kurucz R.L., 1992a, Model Atmospheres for Population Synthesis. In: Barbuy B., Renzini A. (eds.) The stellar population of Galaxies. IAU Symp. 149, Reidel, Dordrecht, p. 225
Kurucz R.L., 1992b, Rev. Mex. Astron. Astrofis. 23, 187
Kroupa P., 1998, MNRAS 298, 231
Maddalena R.J., Morris M., Moscowitz J., Thaddeus P., 1986, ApJ 303, 375
Magazzù A., Martín E.L., Sterzik M.F., et al., 1997, A&AS 124, 449
Marschall L., Mathieu R.D., 1998, AJ 96, 1956
Martín E.L., Claret A., 1996, A&A 306, 408
Martín E.L., 1997, A&A 321, 492
Martín E.L., 1998, AJ 115, 351
Martín E.L., Magazzù A., 1999, A&A 342, 173
Mathieu R.D., 1994, AR&A 32, 465
Mizuno A., Hayakawa T., Yamaguchi N., 1998, ApJ 507, L83
Montmerle T., Koch-Miramond L., Falgarone E., Grindlay J.E., 1983, ApJ 269, 182
Nakano M., McGregor P.J., 1995, In: Chapman J., Cannon R., Harrison S., Hidayat B. (eds.) Future Utilisation of Schmidt Telescopes. ASP Conf. Ser. 84, 376
Neuhäuser R., Sterzik M.F., Torres G., Martín E.L., 1995, A&A 299, L13
Neuhäuser R., 1997, Sci 276, 1363
Neuhäuser R., Torres G., Sterzik M.F., Randich S., 1997, A&A 325, 647
Neuhäuser R., Wolk S., Torres G., et al., 1998, A&A 334, 873
Neuhäuser R., Brandner W., 1998, A&A 330, 29
Pavlenko Y.V., Magazzù A., 1996, A&A 311, 961
Pfeiffer M. J., Frank C., Baumüller D., Fuhrmann K., Gehren T., 1998, A&AS 130, 381
Pinsonneault M.H., Kawaler S.D., Demarque P., 1990, ApJS 74, 501
Preibisch T., Günther E., Zinnecker H., et al., 1998, A&A 333, 619
Queloz D., 1994, In: Davis Philip A.G. (ed.) IAU symposium 167, p. 221
Randich S., Aharpour N., Pallavicini R., Prosser C.F., Stauffer J.R., 1997, A&A 323, 86
Reipurth B., Pedrosa A., Lago M.T.V.T., 1996, A&AS 120, 229
Sanctos Mendes L.T., D'Antona F., Mazzitelli I., 1997, Mem. Soc. Astron. Ital. vol. 68, p. 823
Simkin S.M., 1974, A&A 31, 129
Soderblom D.R., Pendleton J., Pallavicini R., 1989, AJ 97, 539; erratum: vol. 98, 737
Soderblom D.R., Jones B.F., Balachandran S., et al., 1993, AJ 106, 1059
Sterzik M.F., Durisen R.H., 1995, A&A 339, 95
Sterzik M.F., Durisen R.H., Brandner W., Jurcevic J., Honeycutt R., 1997, AJ 114, 1555
Sterzik M.F., Alcalá J.M., Neuhäuser R., Durisen R.H., 1998,In: Burkert A., McCaughrean M. (eds.) The Orion Complex Revisited. Proceedings of the 1997 Rinbgberg Conference on Orion., PASP conf. Ser. in press
Tatematsu K., Umemoto T., Heyer M.H., et al., 1998, ApJS 118, 517
Ventura P., Zeppieri A., Mazzitelli I., D'Antona F., 1998, A&A 331, 1011
Verschueren W., Hensberge H., 1990, A&A 216, 216
Walter F.M., Brown A., Mathieu R.D., Myers P.C., Vrba F.J., 1988, AJ 96, 297
Walter F.M., Alcalá J.M, Neuhäuser R., Sterzik M.F., Wolk S.J., 1999, The low-mass stellar population of the Orion OB1 association and implications for the formation of low-mass stars. In: Protostars & Planets IV, Univ. of Arizona Press, Tucson, in press
Walter F.M., Kuhi L., 1981, ApJ 250, 254
Walter F.M., Wolk S., Sherry W., 1998, In: Donahue R.A., Bookbinder J.A. (eds.) ASP Conf. Ser. 154, The Tenth Cambridge Workshop on Cool Stars, Stellar Systems and the Sun. p. 1793
Wichmann R., Krautter J., Schmitt J.H.M.M., et al., 1996, A&A 312, 439
Wichmann R., Krautter J., Covino E., et al., 1997b, A&A 320, 185
Wichmann R., Covino E., Alcalá J.M., et al., 1999, MNRAS 307, 909
Wiramihardja S. D., Kogure T., Yoshida S., Ogura K., Nakano M., 1989, PASJ 41, 155
Wiramihardja S.D., Kogure T., Yoshida S., et al., 1991, PASJ 43, 27
Wiramihardja S.D., Kogure T., Yoshida S., et al., 1993, PASJ 45, 643